Thus, lysosomes from clathrin-depleted cells are functional. There was no clear difference in the lysosome area profile between cells with and without clathrin (Fig. 5G).

Our data indicate that DKO-R cells express a combined pathway of lysosome biogenesis and turnover that does not show an obligatory dependence on clathrin. It is possible that the DKO-R cell line up-regulated clathrin-independent pathways during the time taken to suppress clathrin expression. Yeast cells expressing a temperature-sensitive clathrin mutant compensate for clathrin inactivation after several hours at the nonpermissive temperature (*31*). But in principle, this question can now be addressed by introducing a similar temperature-sensitive clathrin mutant into DKO-R cells. On the other hand, there is evidence for the existence of alternative pathways of lysosome biogenesis that are present in distinct cell types. For example, LAMP-1 is transported to lysosomes by an AP3-dependent but clathrin-independent mechanism (*32*). The successful targeting of LEP100 in clathrin-depleted DKO-R cells is consistent with this finding. Moreover, lymphocytes and lymphocyte-derived cell lines that lack mannose 6-phosphate receptors (M6PRs) nonetheless retain functional lysosomes (*33, 34*), suggesting that lymphocytes contain an M6PR-independent pathway of lysosome biogenesis. Because DT40 is a lymphocyte cell line, it probably expresses this pathway. If so, the pathway may also be clathrin-independent.

Dense-core lysosomes repeatedly fuse with late endosomes and reform after selective membrane retrieval (*35*). Clathrin has been detected on mammalian lysosomal membranes in vitro, and it has been proposed that clathrin-coated vesicles play a central role in lysosome fusion and recycling (*36*). However, our results can only be reconciled with this view if a reduced recycling rate out of the lysosome caused by clathrin loss is balanced by an exactly proportional reduction in biosynthesis. Clearly, it will now be important to examine the turnover kinetics of individual lysosomal proteins with and without clathrin. But even if clathrin does play a role, it cannot be essential. Our results raise important and unexpected questions about clathrin function, and we have produced flexible experimental models that will enable us to address these issues in cells without interference from endogenous clathrin expression.

References and Notes

1. S. L. Schmid, *Annu. Rev. Biochem.* **66**, 511 (1997).
2. F. M. Brodsky, C.-Y. Chen, C. Knuehl, M. C. Towler, D. E. Wakeham, *Annu. Rev. Cell Dev. Biol.* **17**, 517 (2001).
3. S. K. Lemmon, E. W. Jones, *Science* **238**, 504 (1987).
4. G. S. Payne, T. B. Hasson, M. S. Hasson, R. Schekman, *Mol. Cell. Biol.* **7**, 3888 (1987).
5. T. Ruscetti, J. A. Cardelli, M. L. Niswonger, T. J. O'Halloran, *J. Cell Biol.* **126**, 343 (1994).
6. J.-M. Buerstedde, S. Takeda, *Cell* **67**, 179 (1991).
7. P. Winding, M. W. Berchtold, *J. Immunol. Methods* **249**, 1 (2001).
8. M. Gossen, H. Bujard, *Proc. Natl. Acad. Sci. U.S.A.* **89**, 5547 (1992).
9. E. Sonoda *et al.*, *EMBO J.* **17**, 598 (1998).
10. See supporting data on *Science* Online.
11. F. R. Wettey, data not shown.
12. D. P. Brazil, B. A. Hemmings, *Trends Biochem. Sci.* **26**, 657 (2001).
13. J. Jin *et al.*, *Dev. Cell* **1**, 817 (2001).
14. H. J. Schaeffer, M. J. Weber, *Mol. Cell. Biol.* **19**, 2435 (1999).
15. P. C. Baass, G. M. Di Guglielmo, F. Authier, B. I. Posner, J. J. M. Bergeron, *Trends Cell Biol.* **5**, 465 (1995).
16. G. Carpenter, *Bioessays* **22**, 697 (2000).
17. B. P. Ceresa, S. L. Schmid, *Curr. Opin. Cell Biol.* **12**, 204 (2000).
18. A. Balbis, G. Baquiran, J. J. M. Bergeron, B. I. Posner, *Endocrinology* **141**, 4041 (2000).
19. M. Babst, G. Odorizzi, E. J. Estepa, S. D. Emr, *Traffic* **1**, 248 (2000).
20. G. Evan, T. Littlewood, *Science* **281**, 1317 (1998).
21. A.-O. Hueber, G. Evan, *Trends Genet.* **14**, 364 (1998).
22. T. W. Baba, B. P. Giroir, E. H. Humphries, *Virology* **144**, 139 (1985).
23. E. M. Bennett, S. X. Lin, M. C. Towler, F. R. Maxfield, F. M. Brodsky, *Mol. Biol. Cell* **12**, 2790 (2001).
24. H. Damke, T. Baba, D. E. Warnock, S. L. Schmid, *J. Cell Biol.* **127**, 915 (1994).
25. A. Benmerah *et al.*, *J. Cell Biol.* **140**, 1055 (1998).
26. S. J. Doxsey, F. M. Brodsky, G. S. Blank, A. Helenius, *Cell* **50**, 453 (1987).
27. E. M. van Dam, W. Stoorvogel, *Mol. Biol. Cell* **13**, 169 (2002).
28. M. P. Chang, W. G. Mallet, K. E. Mostov, F. M. Brodsky, *EMBO J.* **12**, 2169 (1993).
29. N. A. Bright, B. J. Reaves, B. M. Mullock, J. P. Luzio, *J. Cell Sci.* **110**, 2027 (1997).
30. J. Lippincott-Schwartz, D. M. Fambrough, *Cell* **49**, 669 (1987).
31. M. Seeger, G. S. Payne, *EMBO J.* **11**, 2811 (1992).
32. A. A. Peden, R. E. Rudge, W. W. Y. Lui, M. S. Robinson, *J. Cell Biol.* **156**, 327 (2002).
33. C. A. Gabel, S. Kornfeld, *J. Cell Biol.* **99**, 296 (1984).
34. F. Dittmer *et al.*, *J. Cell Sci.* **112**, 1591 (1999).
35. J. P. Luzio *et al.*, *J. Cell Sci.* **113**, 1515 (2000).
36. L. M. Traub *et al.*, *J. Cell Biol.* **135**, 1801 (1996).

37. We thank H. Bujard for rtTA vector; T. Nagase for human clathrin heavy-chain cDNA; B. Malissen for plasmid encoding L-histidinol resistance; J. Ortin for plasmid pBSpacΔp encoding puromycin resistance; M. Takata for plasmids containing neomycin- and hygromycin-resistance cassettes; F. M. Brodsky for clathrin heavy-chain monoclonal antibodies (mAbs) X22 for immunofluorescence and TD.1 for blotting; M. S. Robinson for antibodies to γ-adaptin (AP1), α-adaptin (AP2), and D. M. Fambrough for LEP100 mAb. Antibodies to p42/p44 MAPK (MK12) and dynamin were obtained from Transduction Laboratories. Antibodies to Akt, phospho-Akt (Ser^{473}), phospho-Akt substrate, and phospho-p42/44 MAPK (Thr^{202}/Tyr^{204}) were from Cell Signalling Technology, L. Sellers, and A. Tolkovsky. Goat antibody to mouse immunoglobulin G (IgG) conjugated to 10-nm colloidal gold was from British Biocell. HRP- and dye-conjugated antibodies to rabbit and mouse IgG were from Bio-Rad and Molecular Probes, respectively. We thank D. F. Cutler, H. Davidson, M. S. Robinson, P. Shepherd, and A. M. Tolkovsky for helpful discussion and comments on the manuscript and C. Boucher, H. Chatwin, and S. Dornan for help with genomic analysis. Supported by grants from the Biotechnology and Biological Sciences Research Council and the Wellcome Trust (A.P.J. and J.C.H.), the Royal Society (A.P.J.), Deutsche Forschungsgemeinschaft (SFB 243 and 274) and Land Nordrhein-Westfalen through the University of Cologne (J.C.H.), the Medical Research Council (J.P.L.), and a predoctoral Marie Curie Fellowship from the European Commission (F.R.W.). The partial cDNA sequence of chicken clathrin heavy chain has been submitted to the EMBL database under accession number AJ427965. Partial genomic sequences have been submitted to the EMBL database under accession numbers AJ429072, AJ429073, AJ429074, AJ429075, and AJ429076.

Supporting Online Material

www.sciencemag.org/cgi/content/full/297/5586/1521/DC1

Materials and Methods

Figs. S1 to S4

22 May 2002; accepted 18 July 2002

SynCAM, a Synaptic Adhesion Molecule That Drives Synapse Assembly

Thomas Biederer,[1]* Yildirim Sara,[1] Marina Mozhayeva,[1] Deniz Atasoy,[1] Xinran Liu,[1,2] Ege T. Kavalali,[1,3] Thomas C. Südhof[1,2,4]*

Synapses, the junctions between nerve cells through which they communicate, are formed by the coordinated assembly and tight attachment of pre- and postsynaptic specializations. We now show that SynCAM is a brain-specific, immunoglobulin domain–containing protein that binds to intracellular PDZ-domain proteins and functions as a homophilic cell adhesion molecule at the synapse. Expression of the isolated cytoplasmic tail of SynCAM in neurons inhibited synapse assembly. Conversely, expression of full-length SynCAM in nonneuronal cells induced synapse formation by cocultured hippocampal neurons with normal release properties. Glutamatergic synaptic transmission was reconstituted in these nonneuronal cells by coexpressing glutamate receptors with SynCAM, which suggests that a single type of adhesion molecule and glutamate receptor are sufficient for a functional postsynaptic response.

Synapses are specialized intercellular junctions that are assembled when an immature presynaptic terminal contacts a postsynaptic cell. At the site of contact, the presynaptic plasma membrane develops into an active zone, which is where synaptic vesicles undergo exocytosis and release neurotransmitters into the synaptic cleft. On the opposite side of the synaptic cleft, the postsynaptic density contains receptors and signaling molecules

that transduce the neurotransmitter signal into a postsynaptic response (*1*, *2*). How are the tight attachment, precise alignment, and functional differentiation of pre- and postsynaptic membranes achieved? In vertebrates, many synaptic proteins that could participate in these processes have been described—for example the EphrinB/EphB receptor pathway, the neuroligin–β-neurexin cell-adhesion pair, and the cadherin protein family. However, although ephrins perform important functions throughout development (*3*,*4*) and influence synapse assembly (*5*), they are not specifically synaptic cell adhesion molecules. Similarly, the neuroligin–β-neurexin interaction may be important for transsynaptic signaling (*6*–*8*) but is strictly calcium dependent, whereas synaptic cell adhesion is not (*2*, *6*). Moreover, classic cadherins specify synaptic connections but are not part of established junctions (*9*, *10*), whereas protocadherins, although synaptic (*11*), are not evolutionarily conserved. In invertebrates, immunoglobulin domain (Ig domain) proteins perform fundamental functions in synaptic cell adhesion. *Drosophila* fasciclin II and *Aplysia* apCAM are essential for normal synapse formation and maintenance, presumably because they form homophilic extracellular interactions that are coupled to intracellular PDZ-domain proteins (*12*–*16*). However, no equivalent Ig domain protein is known in the vertebrate brain.

Properties of SynCAM. We searched sequence databanks for vertebrate proteins with extracellular Ig domains and an intracellular PDZ-domain protein-interaction sequence, key features of fasciclin II and apCAM. We identified SynCAM (for synaptic cell adhesion molecule), which is relatively small (417 to 456 residues, depending on the splice variant) and evolutionarily conserved (*17*). SynCAM contains an NH_2-terminal signal peptide, three extracellular Ig domains, a single transmembrane region, and a short COOH-terminal cytoplasmic tail (Fig. 1A). SynCAM antibodies reacted with multiple protein bands that were detected only in brain (Fig. 1B). SynCAM mRNA was more widely distributed (*18*), which suggests that posttranscriptional mechanisms restrict expression of SynCAM to the brain. The multiple SynCAM bands are due to complex N-glycosylation, because enzymatic removal of N-linked carbohydrates converted these bands into a single species of about 45 kD, whereas no O-glycosylation of SynCAM was observed (*18*).

SynCAM protein was not detectable in the rat brain at birth, but it increased over the first 3 postnatal weeks, the major period of synaptogenesis in rodents (Fig. 1C). Similar increases were observed for synaptic proteins such as synaptotagmin 1, but VCP (a nonsynaptic protein) remained constant. During the same time period, the N-glycosylation pattern of SynCAM changed (Fig. 1C). In the first 2 weeks, SynCAM was predominantly synthesized as a highly glycosylated ~60-kD form. Thereafter, this form was gradually replaced by a core-glycosylated ~48-kD species that constituted the predominant adult SynCAM form and a cluster of extensively glycosylated species of 60 to 75 kD that were less abundant (Fig. 1C). The level and N-glycosylation pattern of SynCAM varied during development among brain regions (*18*), which suggests that both are regionally regulated.

The cytoplasmic COOH-terminal sequence of SynCAM includes a PDZ-domain protein-interaction sequence that is homologous to that of the synaptic cell-surface proteins neurexins and syndecans, which bind to the PDZ-domain proteins CASK and syntenin (Fig. 1A) (*19*–*22*). Consistent with an interaction of SynCAM with these PDZ-domain proteins, coexpression of SynCAM with CASK recruited CASK from the cytosol to the membrane (Fig. 1D). Furthermore, the cytoplasmic tail of SynCAM strongly bound to CASK and syntenin but not to control PDZ-domain proteins such as PSD-95 (*23*).

Homophilic interaction of SynCAM. To test whether SynCAM functions as a homophilic cell adhesion molecule similar to other Ig domain proteins (*24*), we fused the extracellular sequences of wild-type SynCAM or of mutant SynCAM lacking Ig domains (SynCAMΔIg) to the F_c-domain of human immunoglobulin G and used the resulting IgG fusion proteins in affinity chromatography experiments (*25*). Wild-type extracellular sequences of SynCAM strongly bound endogenous brain SynCAM, whereas mutant

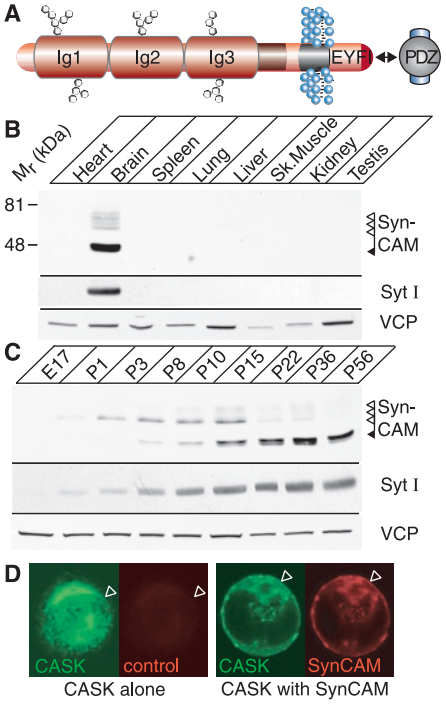

Fig. 1. Properties of SynCAM. (**A**) Structure of SynCAM. Ig1, Ig2, and Ig3 = Ig domains with predicted N-glycosylation sites; EYFI = COOH-terminal Glu-Tyr-Phe-Ile sequence that binds to PDZ domains of CASK, syntenins, and other proteins. (**B**) Brain-specific expression of SynCAM protein. Equal protein amounts (50 μg per lane) from the indicated tissues of 5-week-old rats were probed by immunoblotting with antibodies to SynCAM (top), synaptotagmin 1 (Syt 1) (middle), and VCP (loading control) (bottom). Positions of highly glycosylated (open arrowheads) and core glycosylated (closed arrowheads) SynCAM forms are indicated on the right. (**C**) Developmental regulation of SynCAM expression. Rat brain proteins from the indicated developmental stages (E17 = embryonic day 17; P1 to P56 = postnatal days 1 to 56) were analyzed by immunoblotting as described for (B). (**D**) SynCAM recruits CASK to the plasma membrane. CASK was transfected into 293 cells alone (left) or together with SynCAM (right) and detected by immunocytochemistry (CASK, green; SynCAM, red).

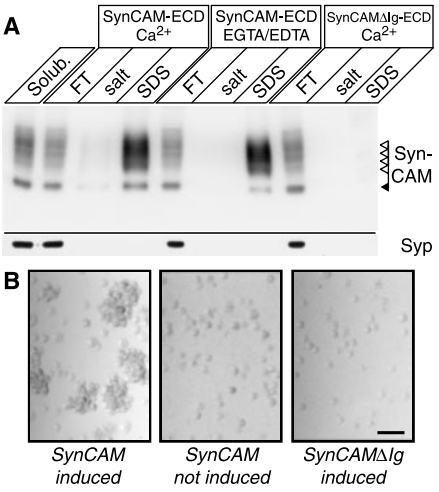

Fig. 2. SynCAM is a homophilic cell adhesion molecule. (**A**) Homophilic binding of SynCAM. Solubilized membrane proteins from rat forebrain (Solub.) were bound to immobilized IgG fusion proteins that contain the full-length extracellular domain (SynCAM-ECD) of SynCAM or a mutant extracellular sequence lacking Ig domains (SynCAMΔIg-ECD) in the presence of Ca^{2+} or EGTA/EDTA. The flow-through (FT) and bound proteins eluted with 0.8 M salt and SDS were analyzed by quantitative immunoblotting with SynCAM antibodies that recognize endogenous but not recombinant SynCAM on the column. A control blot for the synaptic vesicle protein synaptophysin (Syp) is shown at the bottom. (**B**) Cell adhesion by SynCAM. S2 cells were stably transfected with inducible expression vectors encoding full-length SynCAM or the SynCAMΔIg deletion mutant and analyzed with or without induction by bright-field microscopy. Scale bar = 50 μm.

[1]Center for Basic Neuroscience, Departments of [2]Molecular Genetics, and [3]Physiology, and [4]Howard Hughes Medical Institute, University of Texas Southwestern Medical Center, Dallas, TX 75390, USA.

*To whom correspondence should be addressed. E-mail: Thomas.Sudhof@UTSouthwestern.edu (T.C.S.); Thomas.Biederer@UTSouthwestern.edu (T.B.)

SynCAMΔIg did not (Fig. 2A). Binding was resistant to 0.8 M salt and independent of Ca^{2+} (Fig. 2A). Binding was specific for SynCAM because three other neuronal Ig domain proteins (L1, N-CAM, and TAG-1) and abundant synaptic vesicle proteins (synaptophysin 1 and synaptotagmin 1) were not captured (*25*).

To determine whether homophilic binding by SynCAM mediates cell adhesion, we generated stably transfected S2 cells (*6*, *26*) that express full-length SynCAM or SynCAM lacking Ig domains (SynCAMΔIg) under the control of an inducible promoter. When SynCAM expression was induced, the transfected cells aggregated into large clumps, which suggests that SynCAM functions as a homophilic cell adhesion molecule (Fig. 2B). Cell aggregation was independent of Ca^{2+} but was not observed in noninduced cells or in cells expressing SynCAMΔIg. Immunocytochemistry confirmed that both full-length SynCAM and SynCAMΔIg were localized to the plasma membrane in the transfected S2 cells (*27*).

SynCAM is localized to synapses. We examined the localization of SynCAM in brain by subcellular fractionation. SynCAM was highly enriched in synaptic plasma membranes with the synaptic proteins CASK and neuroligin 1 (Fig. 3A) (*28*). Double immunofluorescence labeling of brain sections with antibodies to SynCAM and to synaptophysin, an abundant synaptic vesicle protein, revealed that SynCAM was colocalized with synaptophysin in a punctate synaptic pattern throughout the brain (Fig. 3B) (*29*). These results suggest a synaptic localization for SynCAM, which was confirmed by immunoelectron microscopy that demonstrated SynCAM was present in both pre- and postsynaptic compartments (Fig. 3, C and D). To exclude possible artifacts of immunoelectron microscopy, we quantified the distribution of signals obtained with SynCAM antiserum and with control sera (preimmune serum and SynCAM antiserum that was preabsorbed with the SynCAM antigen) (Fig. 3E) (*30*). Only SynCAM antibodies produced significant synapse staining, whereas control sera did not. Only a subset of synapses were labeled (Fig. 3, B and C), possibly because of the limited sensitivity of immunoelectron microscopy or of the presence of other SynCAMs in the brain (*31*).

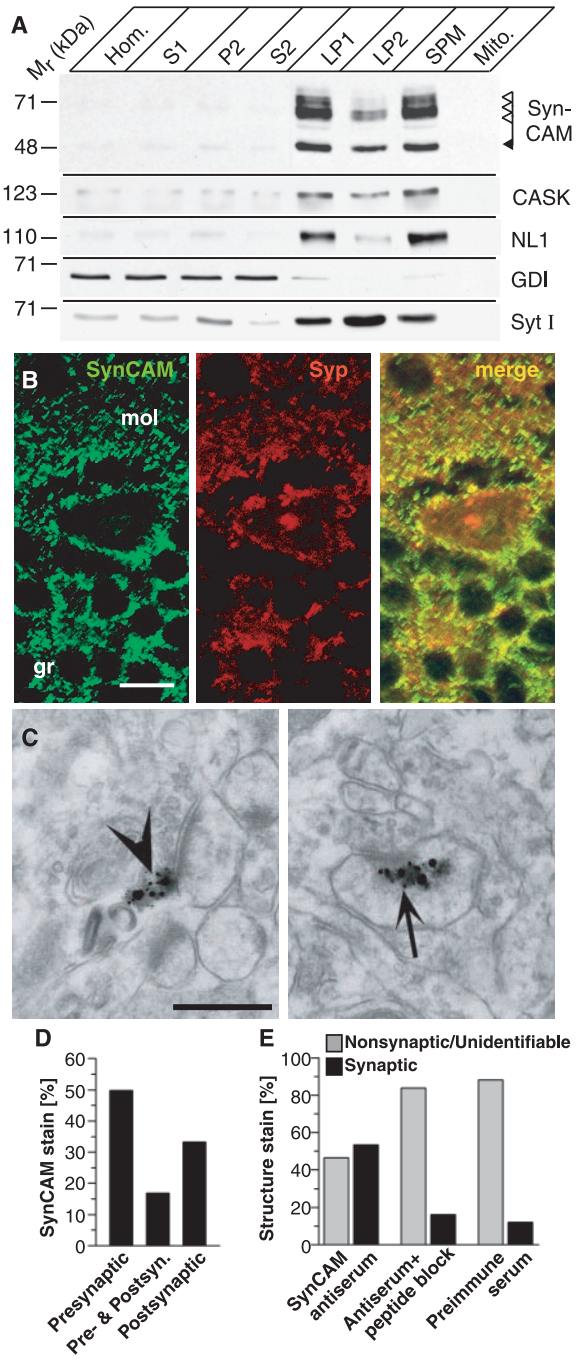

Fig. 3. Localization of SynCAM to synapses. (**A**) Copurification of SynCAM, CASK, and neuroligin 1 (NL1) with synaptic plasma membranes (SPM) during subcellular fractionation. Note that enrichment of SynCAM and neuroligin 1 in synaptic membranes (crude = LP1, purified = SPM) is so high that, at the exposure shown, these proteins are barely detectable in starting materials (Hom. = homogenate, P2 = crude synaptosomes). Equivalent amounts of each fraction (20 μg of protein per lane) were analyzed by immunoblotting. (**B**) Double-immunofluorescence labeling of sections from mouse cerebellum for SynCAM and synaptophysin (Syp). The locations of the molecular (mol) and granule cell layer (gr) are indicated. Scale bar = 10 μm. (**C**) Representative electron micrographs of sections from the hippocampal CA1/CA2 region labeled with SynCAM antibodies. Preembedding immunogold labeling performed with silver enhancement stains presynaptic (arrowhead) and postsynaptic (arrow) sides. Scale bar = 0.5 μm. (**D**) Percentage of SynCAM-positive synapses in which the SynCAM signals were presynaptic or postsynaptic or both in 261 randomly chosen SynCAM-positive synapses. (**E**) Quantitation of the distribution of immunoreactive signals in mouse brain sections obtained with SynCAM antiserum, SynCAM antiserum preadsorbed with the peptide antigen used for immunization, and SynCAM preimmune serum. Locations of immunoreactive particles were classified as synaptic only when they were found in close proximity to a presynaptic vesicle cluster and/or pre- and postsynaptic densities; all other signals were classified as nonsynaptic or unidentifiable (n = 371, 186, and 117 signals for untreated SynCAM antiserum, SynCAM antiserum preabsorbed with the antigen, and preimmune serum, respectively).

SynCAM has a synaptic function. The symmetrical localization of SynCAM on both sides of the synapse suggests a possible role as a homophilic cell adhesion molecule that spans the synaptic cleft. To determine whether SynCAM actually functions at the synapse, we recorded spontaneous miniature synaptic currents (minis) from hippocampal neurons that were transfected with full-length SynCAM, mutant SynCAM lacking Ig domains (SynCAMΔIg), or vector alone (*32*). Overexpression of full-length SynCAM increased the mini frequency two- to threefold [0.81 ± 0.16 Hz (n = 26)] compared with vector-transfected [0.30 ± 0.08 Hz (n = 20)] and nontransfected [0.20 ± 0.06 Hz (n = 6)] neurons. SynCAMΔIg overexpression had no effect [0.28 ± 0.09 Hz (n = 12)]. The increase in mini frequency by full-length SynCAM was statistically significant compared with all other conditions ($P < 0.01$, two-tailed t test) but was not accompanied by a change in mini amplitude (*32*). The mini frequency recorded in a postsynaptic neuron depends primarily on the number of synapses and their release probability, whereas the mini amplitude reflects the abundance of postsynaptic receptors. Thus, SynCAM transfected into the postsynaptic neuron must have induced formation of new synapses or enhanced presynaptic neurotransmitter release at existing synapses on this neuron. This indicates that SynCAM directly affects synaptic function by altering synaptic inputs.

We again used transfected neurons to determine whether SynCAMs or related sequences are required for synapse formation and/or synaptic transmission. But this time we examined the effect of a dominant negative fragment of SynCAM on presynaptic terminals (Fig. 4). We transfected neurons with the isolated full-length cytoplasmic tail of SynCAM (SynCAM C-tail)

or, as a control, a truncated cytoplasmic tail that lacks the COOH-terminal three residues (SynCAM C-tailΔ3). The isolated full-length cytoplasmic tail binds to intracellular PDZ-domain proteins, whereas the truncated cytoplasmic tail does not. As a result, overexpression of full-length cytoplasmic tail but not of the truncated tail is expected to disrupt PDZ-domain interactions of SynCAM or related proteins. Both SynCAM cytoplasmic tail proteins were produced as ECFP (enhanced cyan fluorescent protein, a derivative of green fluorescent protein) fusion proteins to visualize the axons derived from transfected neurons. Possible effects by ECFP itself were controlled for by transfecting ECFP alone. Two days after transfection, we analyzed the presynaptic terminals formed by the axons from transfected neurons by staining terminals with the fluorescent dye FM1-43 (Fig. 4) (*33*, *34*). FM dyes are taken up into, and released from, active nerve terminals in response to synaptic stimulation and thus allow direct visualization and quantifications of synaptic vesicle exo- and endocytosis (*35*).

Presynaptic nerve terminals formed by axons expressing soluble ECFP proteins were clearly identifiable by FM1-43 staining (Fig. 4, A to C). Quantitation of the distance between active terminals revealed a significant decrease in synapse density when the isolated cytoplasmic tail of SynCAM, but not the truncated cytoplasmic tail, was expressed (Fig. 4D). Furthermore, the terminals that were still formed by axons containing the SynCAM cytoplasmic tail were abnormal. The rate of synaptic vesicle exocytosis can be measured in terminals stained with FM1-43, as the kinetics of FM1-43 destaining upon stimulation and the size of the pool of recycling vesicles can be measured as the amplitude of FM1-43 destaining (*36*). Release of FM1-43 stimulated by K^+ depolarization was significantly slower in terminals that expressed full-length SynCAM cytoplasmic tail than in terminals that contained the truncated cytoplasmic tail or ECFP alone (Fig. 4E). In parallel, the average size of the recycling pool of synaptic vesicles decreased almost twofold (Fig. 4F). Together with the changes in mini frequency induced upon overexpression of full-length SynCAM in postsynaptic neurons described above, these results indicate that SynCAM affects synapse formation and function by both a pre- and a postysynaptic action consistent with its pre- and postsynaptic localization.

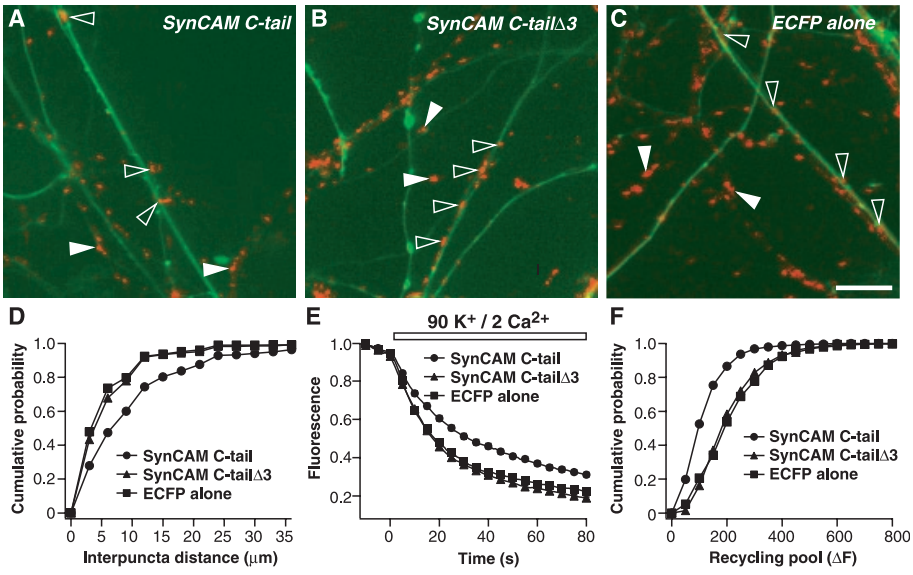

Fig. 4. Effects of transfected intracellular SynCAM sequences on synapse formation in cultured hippocampal neurons. (**A** to **C**) Fluorescence images of axons and synapses from neurons transfected with soluble ECFP fusion proteins (green) and labeled with FM1-43 dye (red). Synapses were labeled with FM1-43 by stimulation with a high concentration of K^+ and then destained by K^+ depolarization to uncover nonspecific residual staining. Images recorded before and after stimulation were subtracted to selectively visualize active presynaptic boutons. Transfected neurons express the full-length (A) or COOH-terminally truncated cytoplasmic tail of SynCAM (SynCAM C-tailΔ3) (B) as soluble ECFP fusion proteins or ECFP alone (C). Scale bar in (C) = 5 μm and applies to all panels. (**D**) Cumulative probability of the distances between FM1-43–labeled synaptic puncta on axons expressing ECFP proteins. The decrease in synapse density on axons containing the full-length SynCAM tail compared with the SynCAM C-tailΔ3 and ECFP alone was statistically significant ($P < 0.001$, Kolmogorov–Smirnov test). (**E**) Destaining rates of FM1-43–labeled synaptic puncta on axons expressing the full-length SynCAM C-tail, SynCAM C-tailΔ3, and ECFP alone. Destaining was triggered by K^+ stimulation. The slower destaining rate of the SynCAM C-tail axons compared with axons expressing SynCAM C-tailΔ3 or ECFP alone was statistically significant ($P < 0.001$, two-tailed t test). (**F**) Cumulative probability histogram of the size of the recycling pool of synaptic vesicles as measured by total FM1-43 staining in synapses formed by axons expressing the full-length cytoplasmic tail of SynCAM, SynCAM C-tailΔ3, or ECFP alone. The difference between terminals expressing the full-length cytoplasmic tail and the two controls was statistically significant ($P < 0.001$, Kolmogorov–Smirnov test). In (D to F), error bars are smaller than the symbols; for (D to F), $n = 537$ for synapses on axons transfected with SynCAM C-tail, $n = 490$ for synapses transfected with SynCAM C-tailΔ3, and $n = 378$ for synapses transfected with ECFP alone.

Expression of SynCAM in nonneuronal cells induces synapse formation. We next examined whether SynCAM has an active role in synapse formation. We transfected 293 cells with wild-type SynCAM, mutant SynCAMΔIg lacking Ig domains, or control proteins. These cells were seeded on top of cultured hippocampal neurons and identified by fluorescence of coexpressed ECFP (*37*). After 3 days of coculture, we analyzed cells by immunocytochemistry with antibodies to synaptic proteins. With all synaptic markers tested, we frequently detected punctate staining of synaptic terminals on the surface of transfected 293 cells expressing SynCAM (Fig. 5, A to C, open arrowheads) but rarely on 293 cells expressing SynCAMΔIg or ECFP alone (Fig. 5D). In vertical cross sections (Fig. 5C), we observed synaptophysin-positive clusters on the cell surface. Quantitation showed that transfected 293 cells expressing full-length SynCAM had about 3 times more clusters than cells expressing mutant SynCAMΔIg or ECFP alone (Fig. 5E), which suggests that induction of presynaptic specializations depended on the Ig domains of SynCAM.

We used the red-shifted fluorescent dye FM5-95 to determine whether the presynaptic specializations induced by SynCAM on 293 cells are capable of synaptic vesicle exo- and endocytosis (*37*). After we labeled cocultures with FM dye, we observed active nerve terminals (Fig. 6A, open arrowheads) over 293 cells expressing wild-type SynCAM but not over 293 cells expressing SynCAMΔIg lacking Ig domains, although stained terminals from interneuronal synapses were present nearby (Fig. 6B, closed arrowheads). Control cells, such as cells expressing mutant SynCAM, occasionally contained networks of neurites on the surface (which explains the infrequent synaptophysin-positive puncta on these cells; see Fig. 5E). However, we detected no terminals with actively recycling vesicles on control cells, which suggests that full-length SynCAM was required for induction of functional presynaptic specializations.

We next measured the rate of exocytosis and the size of the recycling vesicle pool in presynaptic terminals from regular interneuronal synapses and from heterologous synapses on SynCAM-expressing 293 cells by recording the rate (Fig. 6C) and amplitude (Fig. 6D) of FM dye destaining induced by stimulation (*37*). We found no difference between regular synapses and heterologous synapses, which suggests that they are functionally similar. Transfected cells expressing SynCAMΔIg (which lacks Ig domains) or ECFP alone served as

negative controls. Because we detected no obvious staining of synapses with FM dyes on top of these cells, we analyzed the brightest visible spots nearby. For both controls, these spots exhibited only a small decrease in fluorescence (Fig. 6D). Thus, in four different types of experiments—cell adhesion in transfected S2 cells, stimulation of minis in transfected neurons, synapse formation on transfected 293 cells, and induction of quantitatively normal release properties of nerve terminals—the extracellular Ig domains of SynCAM are essential, possibly because they participate in transsynaptic interactions across the synaptic cleft.

Reconstitution of a glutamatergic postsynaptic response. We explored whether presynaptic terminals that contact SynCAM-transfected 293 cells support sustained, localized neurotransmitter release by coexpressing SynCAM with the glutamate receptor GluR2 in 293 cells. SynCAM was transcribed together with soluble ECFP from the same vector, and GluR2 was produced as a green fluorescent protein (GFP) fusion protein, which allowed us to select cells that coexpress SynCAM and GluR2. We cocultured the transfected cells with hippocampal neurons as described above and monitored the 293 cells by whole-cell voltage-clamp recordings (*38*).

Nine of 31 cells coexpressing SynCAM and GluR2 exhibited spontaneous currents (Fig. 7A). We recorded no currents from 293 cells in the absence of neurons. Events occurred at a rate of 2.39 ± 0.63 Hz and were abolished by 6-cyano-7-nitroquinoxaline-2,3-dione (CNQX), which blocks GluR2 glutamate receptors. Control 293 cells expressing either SynCAM or GluR2 alone did not exhibit currents in coculture with neurons (n = 16 for SynCAM, n = 22 for GluR2). Glutamate application onto 293 cells expressing GluR2 triggered large inward currents, confirming that these cells express functional surface receptors (Fig. 7A, bottom right). Current amplitudes recorded in cocultures from 293 cells that coexpressed SynCAM and GluR2 measured 5 to 100 pA but were mostly in the 15- to 35-pA range (Fig. 7B). Rise times varied from 1 to 6 ms, comparable to events from interneuronal synapses in cultures of the same age (Fig. 7C). Confocal imaging of nerve terminals on the transfected 293 cells revealed that GFP-tagged glutamate receptors were often (but not always) concentrated opposite the terminals (Fig. 7D). Because the hippocampal culture system used here forms extended synaptic networks with spontaneous activity (*39*), glutamatergic responses recorded from the transfected 293 cells probably reflected the propagation of this activity to the presynaptic terminals contacting these cells. Consistent with this interpretation, the responses were greatly decreased after tetrodotoxin was applied, which blocks synaptic activity driven by action potentials. Together these results suggest that 293 cells coexpressing SynCAM and GluR2 receptors exhibit postsynaptic glutamatergic responses resembling those of neurons.

Summary. At the synapse, multiple molecules probably contribute to transsynaptic signaling with likely redundancy among molecular pathways. For example, ephrins and cadherins both contribute to synaptic specificity and to the postsynaptic organization of ion channels (*5*, *10*, *40*–*43*). However, many aspects of transsynaptic signaling have remained obscure, especially the mechanism by which neurons signal to each other the need to differentiate a synaptic nerve terminal and the molecular glue that holds pre- and postsynaptic specializations together. SynCAM likely participates in these processes: SynCAM is a homophilic cell adhesion molecule that is present on both sides of the synapse. Overexpression of full-length SynCAM in neurons increased spontaneous synaptic activity, consistent with the notion that SynCAM promoted synapse formation. Conversely, overexpression of the isolated cytoplasmic tail of SynCAM inhibited synapse formation and impaired synaptic release. When produced in nonneuronal cells, SynCAM induced nearby neurons to form synapses onto these cells with release properties that were indistinguishable from those of adjacent interneural synapses. Cell adhesion

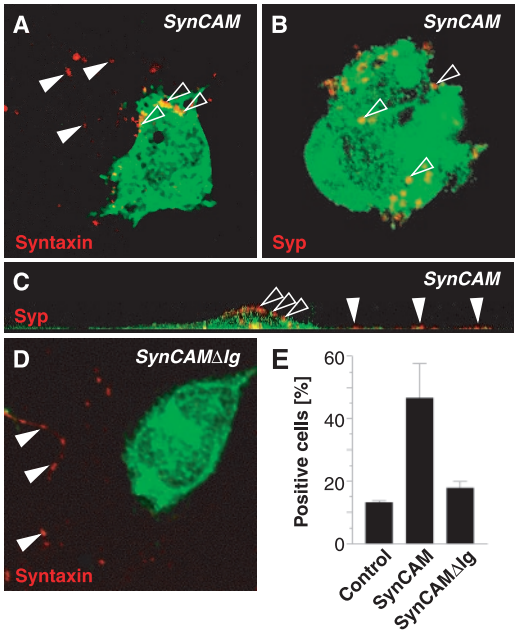

Fig. 5. SynCAM induces synapse formation on transfected 293 cells. Transfected 293 cells that express wild-type SynCAM (**A** to **C**) or mutant SynCAMΔIg (**D**) together with ECFP were seeded onto cultured hippocampal neurons. After 3 days, cocultures were stained with antibodies to syntaxin 1 or synaptophysin 1 (Syp) and examined by fluorescence microscopy (red = syntaxin or synaptophysin; green = ECFP). Open arrowheads point to presynaptic puncta on top of 293 cells; filled arrowheads point to regular interneuronal synapses nearby. (C) A cross section through a transfected 293 cell with nerve terminals forming synapses on top, reconstructed by confocal fluorescence microscopy. (**E**) Quantitation of transfected 293 cells seeded onto hippocampal cultured neurons that contain associated presynaptic terminals (means ± SEMs of percent of transfected cells; n = 188 SynCAM cells; n = 196 SynCAMΔIg cells; n = 143 vector cells in three independent experiments).

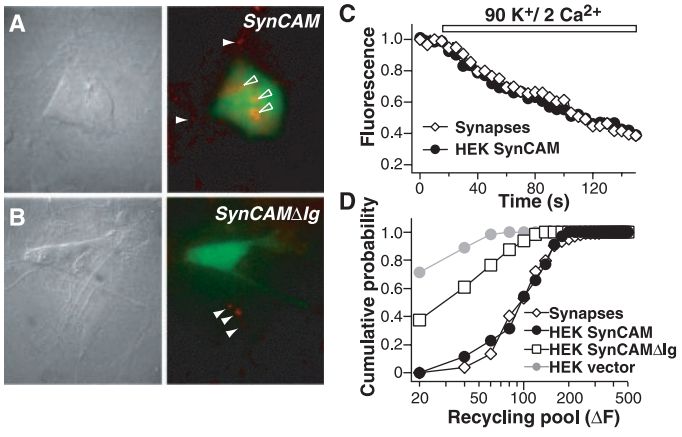

Fig. 6. Synaptic vesicle exocytosis in presynaptic terminals formed on transfected 293 cells. (**A** and **B**) FM5-95 dye staining of active nerve terminals formed on 293 cells that express wild-type SynCAM (A) or mutant SynCAMΔIg (B) together with ECFP after 5 to 7 days of coculture with hippocampal neurons. (Left) Differential interference contrast pictures. (Right) Fluorescence pictures derived by subtracting the FM5-95 images before and after stimulation to selectively visualize active nerve terminals (orange = FM5-95 signal; green = ECFP signal; open and closed arrowheads point to active terminals on and apart from transfected cells, respectively). No active terminals were detected on control transfected cells. (**C**) Average destaining kinetics of presynaptic terminals. Regular interneuronal synapses are compared with synapses formed on transfected 293 cells expressing SynCAM (n = 6, with 10 to 30 puncta per experiment). (**D**) Cumulative probability of the recycling pool of vesicles as measured by the stimulation-dependent FM-fluorescence change (n = 104 interneuronal terminals, n = 35 synapses on SynCAM-expressing 293 cells, n = 64 puncta on SynCAMΔIg-expressing 293 cells; n = 63 on control 293 cells).

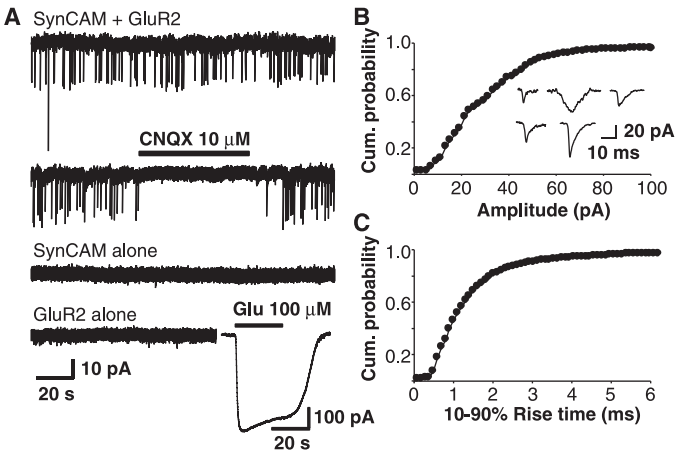

Fig. 7. Reconstitution of glutamatergic synaptic transmission onto transfected 293 cells. (**A**) Representative traces. 293 cells were transfected with SynCAM and GluR2 together or with SynCAM or GluR2 alone and cocultured with hippocampal neurons for 1 to 5 days. Cells were then used for whole-cell recordings in the presence of cyclothiazide to avoid desensitization of glutamate receptors. In the second trace, the glutamate receptor blocker CNQX was applied to verify that the currents observed were glutamatergic. In the bottom right trace, 100 μM glutamate (Glu) was applied to demonstrate that the GluR2 receptors were functional. (**B** and **C**) Cumulative probability of the amplitudes (B) and 10 to 90% rise times (C) of synaptic events recorded from 293 cells expressing SynCAM and GluR2. (Inset) Representative traces of individual events. (**D**) Localizations of active nerve terminals (visualized with FM4-64 shown in red) and GFP-tagged glutamate receptors (GFP-GluR2, shown in green) on transfected 293 cells that coexpress SynCAM with GluR2. (Right) Confocal images are merged with the ECFP labeling of the transfected cells (blue) to illustrate the proximity of receptor clusters to the nerve terminals.

mediated by SynCAM resembles cell adhesion mediated by the β-neurexin–neuroligin pair (*44*), which also induced synapse formation (*8*). The Ca^{2+} independence of SynCAM cell adhesion is consistent with a function as synaptic glue, whereas the β-neurexin–neuroligin interaction is Ca^{2+} dependent (*6*). Conversely, homophilic binding of SynCAM cannot explain the polarized nature of synaptic junctions, which corresponds better to the interaction of β-neurexins with neuroligins or of EphrinB with EphB receptors (*2*).

The fact that heterologous synapses induced in the coculture assay exhibit physiological properties similar to normal brain synapses suggests that a single signal provided by SynCAM is sufficient to instruct the presynaptic terminal for differentiation. Interestingly, the intracellular interactions of SynCAM and β-neurexins are similar in spite of distinct extracellular domains, which indicates that SynCAM and β-neurexins may induce presynaptic differentiation by the same intracellular interactions with PDZ-domain proteins. Thus, inhibition of synapse assembly by the cytoplasmic tail of SynCAM may occur because the tail simultaneously interferes with SynCAM and neurexin signals. Reconstitution of a functional synaptic glutamatergic response in nonneuronal cells expressing SynCAM reveals minimal requirements for synapse assembly and opens up new avenues for studying synaptic function.

References and Notes

1. J. Lisman, K. M. Harris, *Trends Neurosci.* **16**, 141 (1993).
2. T. C. Südhof, in *Synapses,* M. W. Cowan, T. C. Südhof, C. F. Stevens, Eds. (Johns Hopkins Univ. Press, Baltimore, 2001), pp. 275–314.
3. R. Klein, *Curr. Opin. Cell Biol.* **13**, 196 (2001).
4. D. G. Wilkinson, *Nat. Rev. Neurosci.* **2,** 155 (2001).
5. M. A. Takasu, M. B. Dalva, R. E. Zigmond, M. E. Greenberg, *Science* **295**, 491 (2002).
6. T. Nguyen, T. C. Südhof, *J. Biol. Chem.* **272**, 26032 (1997).
7. M. Irie *et al.*, *Science* **277**, 1511 (1997).
8. P. Scheiffele, J. Fan, J. Choih, R. Fetter, T. Serafini, *Cell* **101**, 657 (2000).
9. N. Uchida, Y. Honjo, K. R. Johnson, M. J. Wheelock, M. Takeichi, *J. Cell Biol.* **135**, 767 (1996).
10. J. R. Sanes, M. Yamagata *Curr. Opin. Neurobiol.* **9,** 79 (1999).
11. N. Kohmura *et al.*, *Neuron* **20**, 1137 (1998).
12. C. H. Bailey, M. Chen, F. Keller, E. R. Kandel, *Science* **256**, 645 (1992).
13. M. Mayford, A. Barzilai, F. Keller, S. Schacher, E. R. Kandel, *Science* **256**, 638 (1992).
14. G. W. Davis, C. M. Schuster, C. S. Goodman, *Neuron* **19**, 561 (1997).
15. K. Zito, R. D. Fetter, C. S. Goodman, E. Y. Isacoff, *Neuron* **19**, 1007 (1997).
16. U. Thomas *et al.*, *Neuron* **19**, 787 (1997).
17. See Text and fig. S1 of supporting online material (SOM) on *Science* Online for analysis of the evolutionary conservation and alternative splicing of SynCAM.
18. Antibody production, RNA blotting, tissue-specific and developmentally regulated glycosylation, and deglycosylation experiments are described in the SOM Text and fig. S2.
19. Y. Hata, S. Butz, T. C. Südhof, *J. Neurosci.* **16**, 2488 (1996).
20. Y.-P. Hsueh *et al.*, *J. Cell Biol.* **142**, 139 (1998).
21. J. J. Grootjans *et al.*, *Proc. Natl. Acad. Sci. U.S.A.* **94**, 13683 (1997).
22. T. Biederer, T. C. Südhof, *J. Biol. Chem.* **276**, 47869 (2001).
23. Binding of PDZ-domain proteins to the cytoplasmic COOH terminus of SynCAM was studied by affinity chromatography on immobilized peptides and glutathione *S*-transferase fusion proteins and by cotransfection experiments; see SOM Text and figs. S3 and S4.
24. J. P. Thiery, R. Brackenbury, U. Rutishauser, G. M. Edelman, *J. Biol. Chem.* **252**, 6841 (1977).
25. SynCAM-IgG fusion proteins were produced and used for affinity chromatography with brain extract, and various Ig-domain proteins and abundant synaptic vesicle proteins were used as controls (see SOM Text and fig. S5).
26. P. M. Snow, A. J. Bieber, C. S. Goodman, *Cell* **59**, 313 (1989).
27. Stably transfected S2 cells were used in aggregation assays as described in the SOM Text and fig. S6.
28. Synaptosomes were prepared by differential centrifugation and osmotically lysed; synaptic plasma membranes were then purified by sucrose step gradient centrifugation as described in the Materials and Methods of the SOM.
29. Immunocytochemistry of mouse brain sections by peroxidase staining and double immunofluorescence microscopy is described in the SOM Text and figs. S7 and S8.
30. Preembedding immunoelectron microscopy performed with SynCAM antiserum, with preimmune serum, and with SynCAM antiserum after preabsorption with the antigenic peptide is described in the SOM Text and fig. S9. Both brain sections and cultured hippocampal neurons were examined.
31. At least four closely related SynCAMs are present in mice; see sequence alignment in fig. S10.
32. Mixed hippocampal cultures containing neurons and glia (*39*) were transfected at 5 to 7 days in vitro and analyzed 2 to 3 days after transfection by whole-cell recordings under voltage clamp at −70 mV in the presence of tetrodotoxin as described in the SOM Text and fig. S11.
33. High-density hippocampal cultures (*39*) were transfected at 5 days in vitro, and fluorescence imaging experiments with the dye FM1-43 were performed 2 days after transfection as described in the Materials and Methods of the SOM.
34. Nerve terminals of hippocampal neurons (*39*) were stained with FM1-43 in neuronal transfections (*33*), with red-shifted FM5-95 in cocultures of transfected 293 cells to quantitate release properties (to achieve optical separation between synaptic puncta and the ECFP fluorescence of the transfected cells), and with FM4-64 for colocalization of glutamate receptors [see (*38*)]. FM-dye labeling, recordings, and quantifications of resting and stimulated nerve terminals were done as described in the Materials and Methods of the SOM and fig. S12.
35. W. J. Betz, F. Mao, C. B. Smith, *Curr. Opin. Neurobiol.* **6**, 365 (1996).
36. M. G. Mozhayeva, Y. Sara, X. Liu, E. T. Kavalali, *J. Neurosci.* **22**, 654 (2002).
37. Transfected HEK 293 cells (identified by ECFP expressed from the transfected vector via an IRES sequence) were seeded on cultured hippocampal neurons, cocultured for several days, and analyzed by confocal immunofluorescence microscopy or by fluorescence imaging with the red-shifted dye FM5-95 to quantitate release properties as described in the SOM Text and in fig. S12.
38. 293 cells were cotransfected with various vectors, cocultured with hippocampal neurons, and used for whole cell recordings as described in the SOM. To examine the relative location of glutamate receptor and nerve terminals, cocultures were stained with FM4-64 and viewed by confocal fluorescence microscopy as described in the Materials and Methods of the SOM.
39. E. T. Kavalali, J. Klingauf, R. W. Tsien, *Proc. Natl. Acad. Sci. U.S.A.* **96**, 12893 (1999).
40. G. Feng *et al.*, *Neuron* **25**, 295 (2000).
41. C. C. Garner, J. Nash, R. L. Huganir, *Trends Cell Biol.* **10**, 274 (2000).
42. M. Sheng, D. T. Pak, *Annu. Rev. Physiol.* **62**, 755 (2000).
43. S. Tomita, R. A. Nicoll, D. S. Bredt, *J. Cell Biol.* **153**, F19 (2001).
44. K. Ichtchenko *et al.*, *Cell* **81**, 435 (1995).

45. We thank E. Borowicz, I. Leznicki, and A. Roth for technical assistance and R. Malenka, H. Krämer, F. Schmitz, A. Ho, S. Butz, A. Chubykin, and S. Chandra for advice and reagents. The sequence encoding mouse synCAM1 has been deposited in GenBank (accession number AF539424). E.T.K. is the Effie Marie Cain Endowed Scholar in Biomedical Research at the University of Texas Southwestern Medical Center. Supported by a grant from the NIH to T.C.S. (RO1-MH52804) and a postdoctoral fellowship from the Human Frontier Science Program (to T.B.).

Supporting Online Material
www.sciencemag.org/cgi/content/full/297/5586/1525/DC1
Materials and Methods
SOM Text
Figs. S1 to S12

29 March 2002; accepted 30 July 2002

The Mechanism of Diamond Nucleation from Energetic Species

Y. Lifshitz,[1,*†] Th. Köhler,[2] Th. Frauenheim,[2] I. Guzmann,[3‡] A. Hoffman,[3] R. Q. Zhang,[1] X. T. Zhou,[1] S. T. Lee[1]

A model for diamond nucleation by energetic species (for example, bias-enhanced nucleation) is proposed. It involves spontaneous bulk nucleation of a diamond embryo cluster in a dense, amorphous carbon hydrogenated matrix; stabilization of the cluster by favorable boundary conditions of nucleation sites and hydrogen termination; and ion bombardment–induced growth through a preferential displacement mechanism. The model is substantiated by density functional tight-binding molecular dynamics simulations and an experimental study of the structure of bias-enhanced and ion beam–nucleated films. The model is also applicable to the nucleation of other materials by energetic species, such as cubic boron nitride.

The exciting possible applications of diamond (*1*–*3*) motivated its high-pressure, high-temperature production half a century ago (*4*). Since then, chemical vapor deposition (CVD) methods have been developed to facilitate diamond growth at sub-atmospheric pressures, typically applying a hydrocarbon-hydrogen plasma (<1% hydrocarbon) over a substrate held at ~700° to 800°C. Diamond growth on diamond is relatively well understood and controlled. Diamond growth on non-diamond surfaces requires a nucleation step that is much less understood (*5*) and relies largely on trial and error.

The most controlled diamond nucleation method is biased enhanced nucleation (BEN) (*6*, *7*), in which the substrate is negatively biased to ~100 to 200 V and exposed to the CVD plasma. The impingement of energetic plasma species induces the nucleation of diamond (*8*–*12*). Nucleation can be achieved in a similar way with direct ion beam bombardment (*13*).

Two nucleation sites associated with diamond formation in BEN have been identified: graphitic edges (*8*, *11*, *14*), for randomly oriented diamond, and steps, for heteroepitaxial (oriented) growth on Si (*12*). The actual nucleation process (the formation of a diamond cluster and its subsequent growth to form a stable crystallite) remains unresolved. Here we propose a model of the diamond nucleation process from energetic species (e.g., BEN). Each step in the model is substantiated by experimental data and molecular dynamics (MD) simulation results, as well as reported data and simulations for carbon systems not associated with BEN.

We propose that diamond nucleation via BEN is an internal (bulk) process that occurs in subsurface layers, ~1 to 2 nm below the surface, and advances as follows:

1) Step **a**. Formation of a dense amorphous hydrogenated carbon (a-C:H) phase (~1 to 2 nm thick) via a subplantation (*15*–*17*) process, wherein energetic carbon, hydrocarbon, and hydrogen species bombard the surface and are subsequently stopped and incorporated in subsurface layers. The density of this phase increases with subplantation until it reaches saturation.

2) Step **b**. Spontaneous precipitation of pure sp^3 carbon clusters containing tens of atoms in the a-C:H phase, induced by the "thermal spike" (*15*–*17*) of the impinging energetic species. Most clusters are amorphous, but a few (~1 in 10^4 to 10^6) are perfect diamond clusters. The formation probability of diamond clusters is increased by favorable boundary conditions of nucleation sites

3) Step **c**. Annealing of faults in defective clusters by incorporation of carbon "interstitials" in reactive sites and by hydrogen termination. Carbon interstitials and hydrogen atoms are provided through the subplantation process. Note that the amorphous matrix contains ~20 to 30% of hydrogen by atom (at%H).

4) Step **d**. Growth of diamond clusters to several nm (10^4 to 3×10^4 atoms) through transformation of amorphous carbon to diamond at the amorphous matrix-diamond interface. The transformation is induced by a "preferential displacement" mechanism (*15*–*17*) caused mainly by the impact of energetic hydrogen atoms. In this process, loosely bound amporphous carbon (a-C) atoms move to new diamond positions, leaving the more rigid diamond atoms unchanged. Under typical BEN conditions, the number of energetic hydrogen atoms is two orders of magnitude larger than that of energetic carbon ions, so each carbon atom in the amorphous phase should be bombarded and displaced many times.

Our model differs in two respects from previous attempts to understand the BEN process. First, we suggest that nucleation is a bulk not a surface process, which makes boundary conditions (*15*–*17*) important rather than surface energy effects. We also emphasize that diamond clusters growing on the substrate surface would be annihilated or graphitized by the bombarding energetic species. Second, we assume diamond nucleation to be a highly improbable event, which means the diamond may precipitate even under conditions in which the thermodynamic stability of diamond is lower than that of graphite.

Several major obstacles have previously hampered the elucidation of diamond nucleation mechanisms. First, small diamond clusters of ~30 atoms cannot be observed by experimental techniques, leaving simulation as the only means to observe them. Second, the very low probability of the formation of a perfect diamond cluster (which is still sufficient to facilitate the experimental nucleation densities) requires a large number (>10^4) of cell calculations for it to be observed, calculations that cannot be performed by currently available computers. We overcome these problems by suggesting that the formation of a perfect diamond cluster among many other faulty sp^3 clusters is statistically possible.

Evidence for each of the above steps is found both in new [supporting online material (SOM) Notes 1 to 3] and previously reported data. We first focus on the precursor material (step **a**) in which diamond later precipitates (step **b**) under optimal BEN conditions (*18*). High-resolution transmission electron microscopy (HRTEM) measurements (Fig. 1) prove the precipitation of diamond crystallites in this matrix and the formation of nucleation sites [silicon

[1]Center of Super Diamond and Advanced Films and Department of Physics and Materials Science, City University Hong Kong, Hong Kong SAR. [2]Universitäte/Gesamthochschule Paderborn, D-33095 Paderborn, Germany. [3]Department of Chemistry, Technion, Haifa 32000, Israel.

*To whom correspondence should be addressed. E-mail: apshay@cityu.edu.hk
†On leave from Soreq NRC, Yavne 81800, Israel.
‡Present address: Soreq NRC, Yavne 81800, Israel.